J Comput Electron (2014) 13:606–612
DOI 10.1007/s10825-014-0577-9

# Effects of acceptor dopants on the enhanced piezoelectric potential of ZnO nanowires: limiting free charge-carrier density through neutralizing donors

**Tae Yun Kim · Sang-Woo Kim · Hyoek Kim · Seong Min Kim**

Published online: 1 May 2014


**Abstract** The piezoelectric potential of ZnO can be enhanced using acceptor dopants to neutralize the donor concentrations. In this study, unintentional n-type conductivity is assessed through modeling ZnO nanowires where the activation process of donors ($N_d^+$) is given with a Fermi level ($E_F$) close to the conduction band and followed by the introduction of an acceptor dopant ($N_a^-$) in order to allow $E_F$ to be within the optimum range of $1 \leq E_F \leq 3.2$ eV, which corresponds to the maximum piezoelectric potential calculated. The finite element method simulation reveals that the maximal range of ZnO piezoelectric potential can be obtained due to the intrinsic characteristics of the ZnO nanowire transformed using acceptor dopants, which implies that the limitations on the free-charge carriers (i.e. free-carrier depletion) could reduce the screening effects on the piezoelectric potential. Furthermore, the difference $|N_d^+ - N_a^-|$ is calculated to approach zero near the mid-gap and the energy band structure, which deviates from the normal flat line within the optimal range of $1 \leq E_F \leq 3.2$ eV under the external stress imposed.

T. Y. Kim · S.-W. Kim
Advanced Institute of Nanotechnology (SAINT), Sungkyunkwan University, Suwon 440-746, Republic of Korea

S.-W. Kim
Center for Human Interface Nanotechnology (HINT), School of Advanced Materials Science and Engineering, Sungkyunkwan University (SKKU), Suwon 440-746, Republic of Korea

H. Kim
Photoelectronic Hybrid Research Center, Korea Institute of Science and Technology (KIST), Seoul 136-791, Republic of Korea

S. M. Kim (✉)
CAE Group, Platform Technology Lab, Samsung Advanced Institute of Technology (SAIT), Yongin 449-712, Republic of Korea
e-mail: smkim417@hotmail.com

**Keywords** Acceptor · Dopants · Doping · Piezo-enhancing

## 1 Introduction

Due to their unique structural, biocompatible, and piezoelectric semiconducting properties [1–4], ZnO nanowires (NWs) are considered to be one of the most promising energy-harvesting nanomaterials for potential use in self-powered nanosystems and nanosensors, such as bio and environmental sensors, nanorobotics, micro-electromechanical systems, and portable/wearable electronics. It was recently demonstrated that the harvester energy optimization could be enhanced through reducing the free-charge carrier-induced screening effects, in particular through using piezoelectric semiconducting materials [5,6]. These screening effects result when free electrons in the conduction band are accumulated in a region where a positive piezoelectric potential has been created, which significantly screens this potential. This effect also occurs as a result of the holes in the regions of negative piezoelectric potential. Although the source of n-type conductivity in as-grown ZnO has long been debated [7–9], it is unavoidable to have n-type characteristics naturally occur in ZnO NWs due to their growth environment (oxygen vacancy, hydrogen substitution etc.). However, because these n-type characteristics do not commonly appear in ideal insulating piezoelectric materials such as lead zirconate titanate (PZT) [10], barium titanate ($BaTiO_3$) [11], and polyvinylidene fluoride (PVDF) [12], significant obstacles remain in the fabrication of highly efficient piezoelectric energy harvesters. Furthermore, the unavoidable screening effect hinders the development of more detailed understandings of the mechanism for enhancing the piezoelectric potential.

In this study, continuum-level finite element method (FEM) simulations in which the acceptor dopants were

injected into n-ZnO NWs through activating the energy of acceptors ($\Delta E_A$) were used to compute the piezoelectric potential enhancement. In these reactions, the ionized acceptor neutralizes the ionized donor concentration, thus determining the equilibrium Fermi level ($E_F$) of the ZnO NWs. Due to the charge cancellation effect (i.e. electrons + holes), which reduces the number of free charge carriers and controls the doping, these can be transformed into intrinsic NWs if the number of ionized acceptors and donors is equal. In particular, the intrinsic characteristics can be manipulated through positioning $E_F$ around the mid-gap by controlling the activation process of donors ($N_d^+$) and acceptors ($N_a^-$). The optimum range of Fermi levels ($E_F$) for the enhanced piezoelectric potential can be determined through examining the maximum piezoelectric potential. Correspondingly, these results can also be explained in terms of the free-carrier depletion mechanism (i.e. the electron or hole concentration is reduced significantly). It was also found that within the optimum range, the band structures consisting of the conduction and valence band edges in the NW system along the z-axis deviate from their normal flat lines.

## 2 Simulation details (FEM simulation setup)

In order to calculate the piezoelectric potential distributions in terms of $E_F$, a FEM was used to construct cylindrical ZnO NWs with a diameter of 100 nm and a length of 600 nm. The bottoms of the ZnO NWs were affixed to a substrate and electrically grounded based on the assumption that they would grow epitaxially on the substrate along the c-axis [5]. A constant pressure of $1 \times 10^7$ N/m$^2$ was exerted on the top surface of the NW along its long axis, and the resulting piezoelectric potential at the top was calculated relative to the grounded bottom as a function of $E_F$ ranging from 0 to 3.4 eV (corresponding to the band gap). For the unintentionally introduced n-type character in the ZnO, one single donor level with $\Delta E_D = 35$ meV [5] was used. Furthermore, the activation energy of the acceptors ($\Delta E_A = 130$ meV [13]) was used to numerically describe the p-type character. The following material parameters were used for the simulations in this study: the relative permittivity ($\varepsilon_{ij}$), the coupling matrix ($d_{ij}$), and the compliance matrix ($\varepsilon_{ij}^E$) for ZnO [14].

## 3 Results and discussion

Figure 1 presents a schematic of the energy band structure where the position of $E_F$ is dependent on the density of the free carriers at the conduction band or valance band. For the highly n-doped ZnO (Fig. 1a), $E_F$ is positioned close to the conduction band with a shallow donor level ($\Delta E_D$). However, if the acceptor dopant is introduced, $E_F$ can be positioned near the mid-gap (Fig. 1b). Furthermore, $E_F$ can be further positioned toward the valance band if the acceptor density is too much compared with the density of donors as shown in Fig. 1c. For the as-grown ZnO NWs that are usually highly n-doped, the ionized donor is equal to the electron density due to the neutrality condition such as $N_d^+ \approx n$, where $N_d^+ = \frac{N_d}{1+2e^{(E_F-E_C+\Delta E_D)/kT}}$ and $n = N_C e^{(E_F-E_C)/kT}$. Therefore,

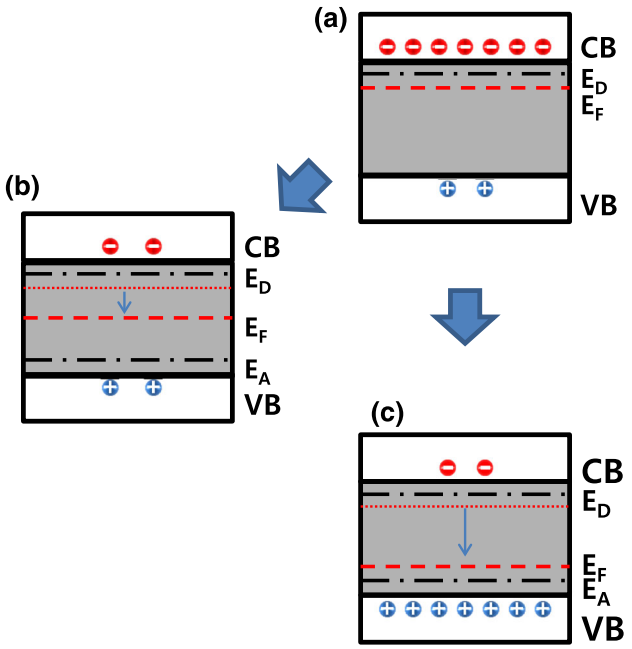


**Fig. 1** **a** Schematic band structure of ZnO nanowire for highly n-doped scenario where $E_F$ is close to the conduction band (CB) and $E_D$ is the donor energy level; in this scenario, $\Delta E_D$ is 35 meV. **b** Band structure where the acceptor dopant is added. $E_A$ is the acceptor energy level; in this scenario, $\Delta E_A = 130$ meV. The $E_F$ is positioned near the mid-gap due to the free-carrier cancellation. **c** Band structure where $E_F$ is positioned closer to the valance band as a result of the significant increase in the acceptors introduced

$$N_d^+ = \frac{N_d}{1 + 2\left(\frac{n}{N_C}\right)e^{\Delta E_D/kT}} = n, \tag{1}$$

$$N_d = n\left[1 + \frac{2n}{N_C}e^{\Delta E_D/kT}\right], \tag{2}$$

$$n = \frac{1}{4}e^{-\Delta E_D/kT}\left\{-N_C + \sqrt{N_C}\sqrt{N_C + 8e^{\Delta E_D/kT}\cdot N_d}\right\}. \tag{3}$$

Here, if $n = N_C e^{(E_F-E_C)/kT}$ is substituted into Eq. (3), then $E_F$ can be solved as follows:

$$E_F = E_C + kT \times \left\{ ln\left[\frac{-N_C + \sqrt{N_C}\sqrt{N_C + 8e^{\Delta E_D/kT}\cdot N_d}}{4N_C}\right] - \frac{\Delta E_D}{kT}\right\}, \quad (4)$$

where $E_C$ is the conduction band edge, $N_C$ is the effective state density of the conduction band, $N_d$ is the donor concentration, $\Delta E_D$ is the activation energy of the donors, $k$ is the Boltzmann constant, and $T$ is the temperature. Conversely, for highly p-doped ZnO NWs, the ionized acceptor is equal to the hole density due to the neutrality condition of $N_a^- \approx p$, where $N_a^- = \frac{N_a}{1+4e^{(E_V-E_F+\Delta E_A)/kT}}$ and $p = N_V e^{(E_V-E_F)/kT}$. Therefore,

$$N_a^- = \frac{N_a}{1+4\left(\frac{p}{N_V}\right)e^{\Delta E_A/kT}} = p, \quad (5)$$

$$N_a = p\left[1+\frac{4p}{N_V}e^{\Delta E_A/kT}\right], \quad (6)$$

$$p = \frac{1}{8}e^{-\Delta E_A/kT}\left\{-N_V + \sqrt{N_V}\sqrt{N_V + 16e^{\Delta E_A/kT}\cdot N_a}\right\}. \quad (7)$$

Here, if $p = N_V e^{(E_V-E_F)/kT}$ is substituted into Eq. (7), then $E_F$ can be solved as follows:

$$E_F = E_V - kT \times \left\{ ln\left[\frac{-N_V + \sqrt{N_V}\sqrt{N_V + 16e^{\Delta E_A/kT}\cdot N_a}}{8N_V}\right] - \frac{\Delta E_A}{kT}\right\}, \quad (8)$$

where $E_V$ is the valance band edge, $N_V$ is the effective state density of the valence band, $N_a$ is the acceptor concentration, and $\Delta E_A$ is the activation energy of the acceptor. Finally, for an intermediately doped case where both the donor and acceptor dopant coexist, the following neutrality condition is satisfied:

$$p + N_d^+ = n + N_a^-. \quad (9)$$

Equation (9) can be then rewritten as follows:

$$N_V e^{(E_V-E_F)/kT} + \frac{N_d}{1+2e^{(E_F-E_C+\Delta E_D)/kT}} = N_C e^{(E_F-E_C)/kT} + \frac{N_a}{1+4e^{(E_V-E_F+\Delta E_A)/kT}}, \quad (10)$$

$$\frac{N_d}{1+2e^{38.5(E_F-3.36)}} \approx \frac{N_a}{1+4e^{38.5(0.13-E_F)}} + N_C e^{38.5(E_F-3.4)}. \quad (11)$$

Thus, $E_F$ can be solved numerically based on Eq. (11).

Using the Voigt–Nye notation [5], the equation for the piezoelectric field can be written as follows:

$$\nabla\cdot D = \frac{\partial}{\partial x_i}\left(e_{iq}\varepsilon_q + \kappa_{ik}E_k\right)$$

$$= ep - en + eN_d^+ \left(N_d^+ \gg N_a^-\right), \quad (12)$$

$$= ep - en + eN_d^+ - eN_a^- : \text{Intermediate doping}, \quad (13)$$

$$= ep - en - eN_a^- \left(N_d^+ \ll N_a^-\right), \quad (14)$$

$$= ep - en \left(N_d^+ = N_a^-\right), \quad (15)$$

where $E$ is the electric field, $D$ is the electric displacement, $\kappa_{ik}$ is the dielectric constant, $e_{iq}$ is the piezoelectric constant, $\varepsilon_q$ is the strain, $p$ is the hole concentration in the valence band, $n$ is the electron concentration in the conduction band, $N_d^+$ is the ionized donor concentration, and $N_a^-$ is the ionized acceptor concentration. Through the introduction of a piezoelectrically induced polarization ($\rho^R = -\nabla\cdot e_{kq}\varepsilon_q\hat{i}_k$ corresponding to a piezoelectric charge), Eqs. (12)–(15) can be solved for the piezoelectric potential ($\varphi$), as follows:

$$\kappa_{ik}\frac{\partial^2}{\partial x_i\partial x_k}\varphi = -\left(\rho^R + ep - en + eN_d^+\right)\left(N_d^+ \gg N_a^-\right), \quad (16)$$

$$= -\left(\rho^R + ep - en + eN_d^+ - eN_a^-\right) : \text{Intermediate doping}, \quad (17)$$

$$= -\left(\rho^R + ep - en - eN_a^-\right)\left(N_d^+ \ll N_a^-\right), \quad (18)$$

$$= -\left(\rho^R + ep - en\right)\left(N_d^+ = N_a^-\right). \quad (19)$$

The redistribution of the free-charge carriers (electrons and holes) under the thermodynamic equilibrium is given by Fermi-Dirac statistics [5,13]:

$$n \approx 2\left(\frac{2\pi m_e kT}{h^2}\right)^{3/2} e^{\left(\frac{E_F-E_C(\vec{x})}{kT}\right)}, \quad (20)$$

$$p \approx 2\left(\frac{2\pi m_h kT}{h^2}\right)^{3/2} e^{\left(\frac{E_V(\vec{x})-E_F}{kT}\right)}, \quad (21)$$

where the locations of the conduction band edge ($E_C(\vec{x})$ and the valence band edge ($E_V(\vec{x})$) are both a function of the coordinates, and the effective masses of the conduction band electrons and valence band holes are given by $m_e$ and $m_h$, respectively. Finally, the activation processes of the donors and acceptors are given by:

$$N_d^+ \approx \frac{n}{1+2e^{(E_F-E_D)/kT}}\left(N_d^+ \gg N_a^-\right), \quad (22)$$

$$N_a^- \approx \frac{p}{1+4e^{(E_A-E_F)/kT}}\left(N_d^+ \ll N_a^-\right), \quad (23)$$

$$N_d^+ - N_a^- \cong \frac{n}{1+2e^{(E_F-E_D)/kT}} - \frac{p}{1+4e^{(E_A-E_F)/kT}}, \quad (24)$$

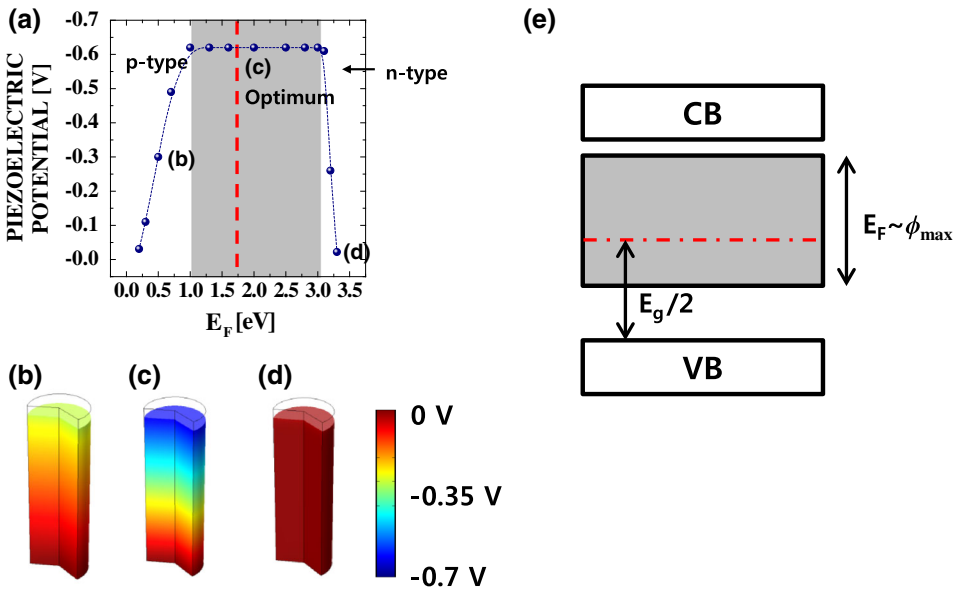


**Fig. 2** **a** Piezoelectric potential calculated at the top surface of the ZnO NWs under uniaxial compression as a function of the equilibrium Fermi level ($E_F$). At each side of region, it can be seen that the piezoelectric potential is significantly reduced due to the free-carrier screening effects. **b–d** Piezoelectric potential distribution along the z-axis corresponding to each point of the main plot. The region 1.0 eV $< E_F <$ 3.2 eV (*grey square*) is denoted as the optimum region where the maximum piezoelectric potential is possible. **e** Schematic band structure of ZnO nanowire where the optimum range of $E_F$ (1.0 eV $< E_F <$ 3.2 eV) corresponding to the maximum piezoelectric potential is indicated as a *grey box* between the conduction and valence bands (Color figure online)

where $E_D$ and $E_A$ are the position-dependent donor and acceptor energy levels, respectively [5,13]. In Eqs. (12)–(19), the right-hand sides are functions of $E_F$ [see Eqs. (20)–(24)]. Here, the donor ($N_d$) and acceptor ($N_a$) concentrations are approximated as $n$ and $p$, respectively.

Figure 2a illustrates the piezoelectric potential calculated at the top surface of the ZnO NWs under compression as a function of $E_F$. On each side, it can be seen that the piezoelectric potential is significantly reduced due to the free-carrier screening effects. In Fig. 2a, the potential can be divided into three regions: (i) in the vicinity of the region ($E_F < \sim 1.0\,eV$), the piezoelectric potential increases linearly until it reaches its saturation value of $-0.63$ V; (ii) after this, the piezoelectric potential value remains constant until $E_F = 3.2$ eV (this region, corresponding to 1.0 eV $< E_F <$ 3.2 eV, is called the optimum region due to its maximal piezoelectric potential); and (iii) finally, in the region close to the conduction band, the piezoelectric potential drops exponentially due to the electronic screening effects. As a result of the differing degeneracy factors and activation processes for the donors and acceptors, each region exhibits asymmetric behavior (the activation energy of the donors is $\Delta E_D = 35$ meV [5], whereas that of the acceptors is $\Delta E_A = 130$ meV [13]). Note that Fig. 2b–d present the piezoelectric potential distributions along the z-axis corresponding to each point (b), (c), and (d) in Fig. 2a. Figure 2(e) presents a schematic band structure at the ZnO structure where the optimum region of $E_F$ (1 eV $\leq E_F \leq$ 3.2 eV) is depicted, which corresponds to the maximum piezoelectric potential ($\phi_{max}$) calculated. Note that the central line indicates the mid-gap ($E_g/2$) between the conduction band and valence band.

In Fig. 3a, the electron concentration distribution is plotted along the z-coordinate as a function of $E_F$. It can be seen that the concentration profile for the ZnO NWs ($E_F = 3.2$ eV) was significantly reduced when the Fermi level shifted into the region as shown in Fig. 2e ($E_g/2 < E_F < 3.2$ eV); this was caused by the cancellation between the free-charge carriers (electrons and holes), particularly the holes that were generated by the introduction of the acceptor dopants. Note that the electron concentration near the top surface of the NWs decreased due to electrostatic repulsion from the generated negative piezoelectric potential. In the reverse case, the electrons accumulated near the bottom of the ZnO due to the local positive piezoelectric potential (i.e. electrostatic attraction) generated under the uniaxial compression along the c-axis (compression $T_Z = -10^7$ N/m$^2$). Note that the region of $E_g/2 < E_F < 3.2$ eV, as shown in Fig. 2e, clearly reveals the electron-depletion mechanism that is correlated to the enhanced piezoelectric potential shown in Fig. 2a. Figure 3b is an ionized donor concentration ($N_d^+$) profile along the z-axis as a function of $E_F$ and the pattern is similar

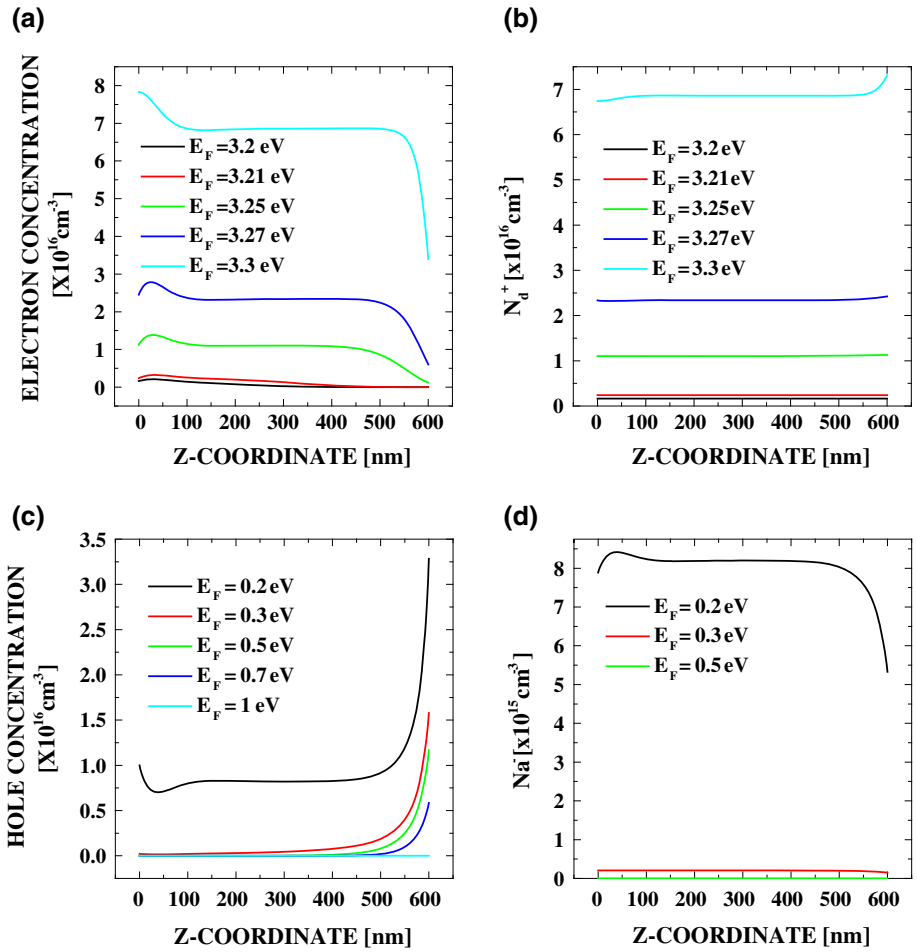


**Fig. 3** **a** Electron and **c** hole concentration distribution along the z-coordinate under compression as a function of the equilibrium Fermi level ($E_F$). As a result of the free-carrier depletion, the concentration profile for each free carrier is significantly reduced when the Fermi level is shifted to $E_F = 3.2$ eV for electrons and to $E_F = 1$ eV for holes. Note that due to the free-carrier depletion, the concentration profiles for the **b** ionized donor concentration ($N_d^+$) and **d** ionized acceptor concentration ($N_a^-$) were also significantly reduced, which satisfies the neutrality conditions including $n \approx N_d^+$ and $p \approx N_a^-$ for highly doped scenarios

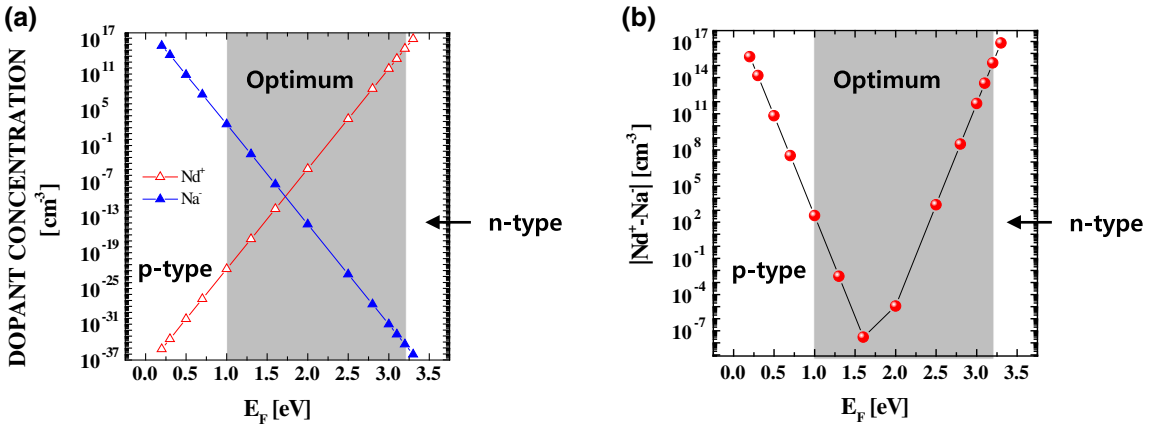


**Fig. 4** **a** Calculated ionized donor ($N_d^+$) and ionized acceptor ($N_a^-$) concentrations as a function of $E_F$ with a neutrality condition of $-n + p = N_a^- - N_d^+$. Note that the shaded area indicates the optimum region where the maximum piezoelectric potential is maintained as seen in Fig. 2a. **b** Calculated dopant difference between $N_d^+$ and $N_a^-$, which approaches zero near the mid-gap within the optimum range

to the electron concentration profile due to the neutrality condition ($n \approx N_d^+$). In contrast, for the hole concentration distribution (Fig. 3c), it can be seen that the concentration profile was also reduced when the Fermi level rose from the valence band and went into the region of 1 eV $< E_F < E_g/2$. This was caused by the cancellation between the hole carriers (p-type) and electrons, and the electrons were generated through the introduction of the donor dopant, which is the opposite situation to that in the electron concentration profile explained previously. Note that the hole concentration on the top of the

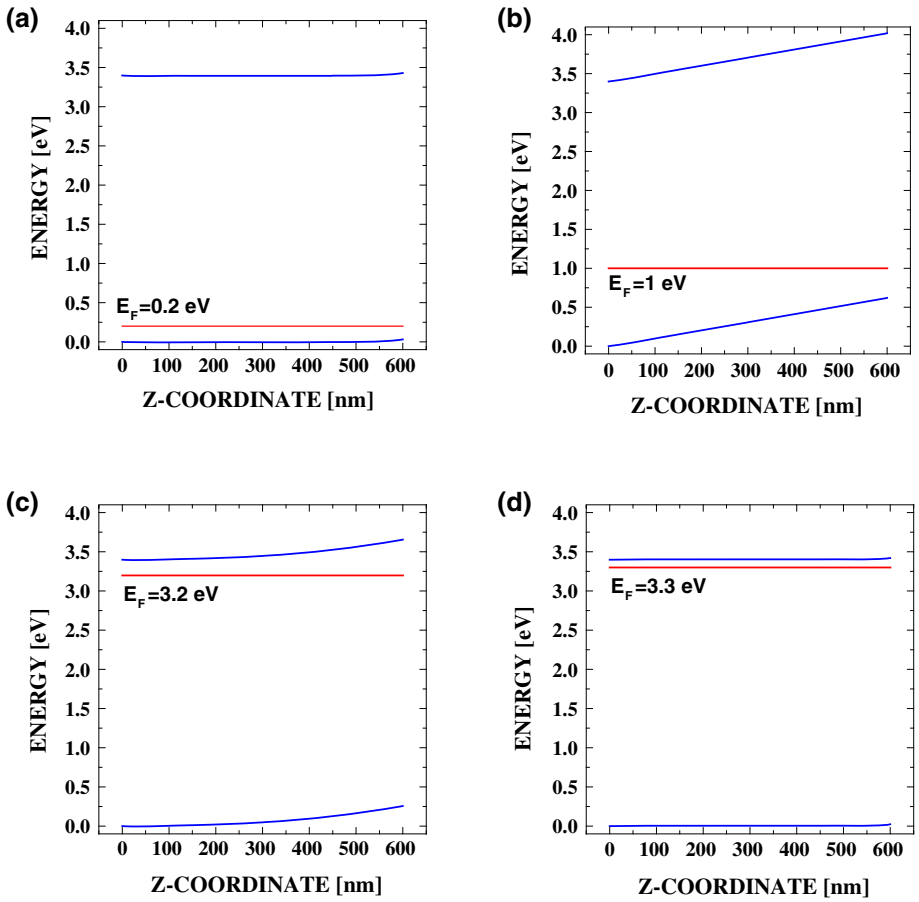


**Fig. 5** Calculated band structures of the ZnO nanowires along the z-coordinate under compression with different $E_F$ values. If $E_F$ is close to **a** the valence band or **d** the conduction band, the two bands (conduction and valence) are flat over the compressed nanowire. However, if $E_F$ is within the optimum range (**b** and **c**), the conduction and valence bands deviate from the flat line along the z-coordinate under external compression

NWs increased due to the electrostatic attraction that was induced by the negative piezoelectric potential and vice versa on the bottom of NWs, which is clearly seen in Fig. 3c. The ionized acceptor concentration ($N_a^-$) is also plotted along the z-axis as a function of $E_F$ and it almost satisfies the neutrality condition ($p \approx N_a^-$) as shown in Fig. 3d. The activated donor ($N_d^+$) or acceptor ($N_a^-$) concentration at the top of the ZnO NWs exhibited the opposite behavior to the electron ($n$) and hole ($p$) density due to the opposite charged states. For example, if the negative piezoelectric potential was induced on top of the NWs via external compression, the electrons were then depleted but the positively ionized donor centers remained to be accumulated for the n-type scenario and vice versa for the p-type scenario. Furthermore, the activated acceptor ($N_a^-$) was one order of magnitude lower than the hole concentration. This is potentially results from the degeneracy factor of 4 in the activation process of the acceptor differed to that of the donor case, where the degeneracy factor was 2.

Figure 4a presents the calculated dopant concentrations ($N_d^+$ and $N_a^-$) as a function of $E_F$ that satisfy the neutrality condition of $-n + p = N_a^- - N_d^+$. Note that the shaded area indicates the optimum region where the piezoelectric potential was enhanced and maximized (Fig. 2a). This plot quantitatively demonstrates how much acceptor dopant should be added for the NWs to obtain intrinsic-like properties from the highly n-typed dopant (i.e. $N_d \approx 10^{17}$ cm$^{-3}$). Figure 4b presents the difference between $N_d^+$ and $N_a^-$ that approaches zero within the optimum range, including the intrinsic regions corresponding to the piezoelectric potential maximum. Clearly, $N_d^+$ or $N_a^-$ is dominant at the edge of the plot, which leads to abundant free carriers, which in turn ultimately screens the piezoelectric potential. However, if $E_F$ is in the optimum region, the reduction of free carriers enhances the piezoelectric potential.

Figure 5 presents the calculated band structure of the ZnO nanowires along the z-coordinate with different $E_F$ values under compression. It was found that either $E_F$ was close to the conduction band or valence band, and the two bands changed only slightly along the z-coordinate as shown in Fig. 5a and d, respectively. In contrast, if $E_F$ was within the optimum range, the conduction and valence bands were not flat over the compressed nanowires as shown in Fig. 5b and c, respectively. This results from the conduction or valence band edge ($E_{C/V}$) being the sum of the piezoelectric potential ($\phi$) and the energy band edge of an un-deformed nanowire ($E_{C_0/V_0}$) as a reference where the potential is the coordinate-

dependent function such as $E_{C/V} = E_{C_0/V_0} - e\phi$. When $E_F$ was close to either the conduction band or valence band, the piezoelectric potential was screened by the free carriers, and then $E_{C/V} \approx E_{C_0/V_0}$. However, in the optimum range, the piezoelectric potential could influence the energy band edge.

## 4 Conclusions

In this paper, an analytically derived mechanism for enhancing the piezoelectric potential was described through the introduction of acceptor dopants. Using FEM simulations, it was determined that controlling the activation process of $N_d^+$ and $N_a^-$ would allow for the tuning or maximizing of an optimal range for the piezoelectric potential in order to limit and control the charge-carrier concentrations. The computational results also validate the correlation between the free-carrier depletion and enhanced piezoelectric potential with sloped band structures along the z-coordinate under external stresses [15,16].

**Acknowledgments** This work was supported by the Computational Energy Harvesting (CEH) project in Samsung Advanced Institute of Technology. This research was supported by National Research Foundation of Korea (NRF) grants funded by the Ministry of Science, ICT & Future Planning (2009-0083540) and the Energy International Collaboration Research & Development Program of the Korea Institute of Energy Technology Evaluation and Planning funded by the Ministry of Knowledge Economy (2011-8520010050).

## References

1. Wang, Z.L., Song, J.H.: Piezoelectric nanogenerators based on zinc oxide nanowire arrays. Science **312**, 242–246 (2006)
2. Wang, Z.L.: ZnO nanowire and nanoblet platform for nanotechnology. Mater. Sci. Eng. R **64**, 33–71 (2009)
3. Hu, Y., Zhang, Y., Xu, C., Lin, L., Snyder, R.L., Wang, Z.L.: Self-powered system with wireless data transmission. Nano Lett. **11**, 2572–2577 (2011)
4. Wang, Z.L.: Self-powered nanosensors and nanosystems. Adv. Mater. **24**, 280–285 (2012)
5. Gao, Y., Wang, Z.L.: Equilibrium potential of free charge carriers in a bent piezoelectric semiconductive nanowire. Nano Lett. **9**, 1103–1110 (2009)
6. Romano, G., Mantini, G., Carlo, A.D., D'Amico, A., Falconi, C., Wang, Z.L.: Piezoelectric potential in vertically aligned nanowires for high output nanogenerators. Nanotechnology **22**, 465401–465406 (2011)
7. Kröger, F.A.: The Chemistry of Imperfect Crystals. North-Holland, Amsterdam (1974)
8. Look, D.C., Hemsky, J.W., Sizelove, J.R.: Residual native shallow donor in ZnO. Phys. Rev. Lett. **82**, 2552–2555 (1999)
9. Tomlins, G.W., Routbort, J.L., Mason, T.O.: Zinc self-diffusion, electrical properties, and defect structure of undoped, single crystal zinc oxide. J. Appl. Phys. **87**, 117–123 (2000)
10. Xu, S., Hansen, B.J., Wang, Z.L.: Piezoelectric-nanowire-enabled power source for driving wireless microelectronics. Nat. Commun. **1**, 93–98 (2010)
11. Hu, J., Suryavanshi, A.P., Yum, K., Yu, M.F., Wang, Z.Y.: Voltage generation from individual $BaTiO_3$ nanowires under periodic tensile mechanical load. Nano Lett. **7**, 2966–2969 (2007)
12. Cha, S.N., Kim, S.M., Kim, H.J., Ku, J.Y., Sohn, J.I., Park, Y.J., Song, B.G., Jung, M.H., Lee, E.K., Choi, B.L., Park, J.J., Wang, Z.L., Kim, J.M., Kim, K.: Porous PVDF as effective sonic wave driven nanogenerators. Nano Lett. **11**, 5142–5147 (2011)
13. Ming-Pei, L., et al.: Piezoelectric nanogenerator using p-type ZnO nanowire arrays. Nano Lett. **9**, 1223–1227 (2009)
14. Piezoelectric ZnO Property is Supported by the Material Library in COMSOL Multiphysics Package v. 4.2(a)
15. Kim, S.M., Kim, H., Nam, Y., Kim, S.: Effects of external surface charges on the enhanced piezoelectric potential of ZnO and AlN nanowires and nanotubes. AIP Adv. **2**, 042174–042178 (2012)
16. Sohn, J.I., Cha, S.N., Song, B.G., Lee, S., Kim, S.M., Ku, J., Kim, H.J., Park, Y.J., Choi, B.L., Wang, Z.L., Kim, J.M., Kim, K.: Engineering of efficiency limiting free carriers and an interfacial energy barrier for an enhancing piezoelectric generation. Energy Environ. Sci. **6**, 97–104 (2013)